Dalton Transactions

ROYAL SOCIETY OF CHEMISTRY

COMMUNICATION

View Article Online
View Journal | View Issue





Cite this: *Dalton Trans.*, 2020, **49**, 31

Received 10th November 2019,
Accepted 26th November 2019

DOI: 10.1039/c9dt04354c

rsc.li/dalton

# One-step electrodeposition of the MOF@CCQDs/NiF electrode for chiral recognition of tyrosine isomers†

Ying Hou,[a] Zhaoxuan Liu,[a] Lei Tong,[a] Lu Zhao,[a] Xuan Kuang,*[a] Rui Kuang*[b] and Huangxian Ju[a]

**Electrochemical enantiorecognition of tyrosine (Tyr) isomers using a MOF@CCQDs/NiF electrode prepared by electrodepositing a metal–organic framework (MOF) and chiral carbon quantum dots (CCQDs) on Ni foil is reported. MOF@CCQDs/NiF not only shows highly selective, sensitive and quantitative analysis towards Tyr enantiomers but also presents the ability to determine L-Tyr% in racemic mixtures. This proposed that chiral sensors could be considered for practical applications in the field of Tyr related medical recognition.**

Enantiomeric recognition remains of paramount importance in stereospecific synthesis, pharmaceuticals, pesticides and food additives,[1] on account of different physiological responses to different chiral isomers.[2] Amino acids are fundamental structural molecular building blocks of life, and exist in the form of two enantiomers. L-Amino acids are considered the elementary unit of proteins in humans.[3] Although D-amino acids are present in small amounts, they may have negative effects on human health.[4] Thus, chiral discrimination of amino acids can provide a better understanding of their biological and physiological functions and facilitate the development of drug screening. In comparison with traditional methods, electrochemical chiral sensing and detection with high sensitivity, simple operation and low cost is an emerging technique that avoids complicated pretreatment and expensive chiral selectors.[5] The construction of chiral interfaces is considered to be one of the most challenging tasks for electrochemical chiral sensing.[6]

Homochiral metal–organic frameworks (HMOFs) with diverse architectures, record-high surface areas and selective adsorption affinity make them attractive as electrochemical sensors.[7] However, complex and costly enantiopure organic ligands greatly hinder the further applications of most reported HMOFs in practice. Therefore, enabling chiral sensing by chiral modification of achiral MOFs will significantly extend MOF applications in chiral discrimination.

Chiral carbon quantum dots (CCQDs), as novel green nanomaterials, offer us an exciting opportunity for chiral discrimination. However, to date, much of CCQD research has focused on enantioseparation and enantiomeric determination by chemiluminescence technology. For example, Zhang and coworkers illustrated (*S*)-1810-QDs having a highly chiral-selective fluorescence response toward (1*R*,2*S*)-2-amino-1,2-diphenyl ethanol, and successfully separated the racemic solution of (1*S*,2*R*)-2-amino-1,2-diphenyl ethanol and (1*R*,2*S*)-2-amino-1,2-diphenyl ethanol using the membrane of (*S*)-1810-QDs. Copur *et al.* synthesized CCQDs having nanoscale chirality from optically pure L-cysteine and embedded them into nanopaper for photoluminescence sensors,[8] and the CCQDs showed an enantioselective response towards lysine enantiomers. To the best of our knowledge, CCQDs were rarely adopted in electrochemical enantioselective recognition.[9,10] Thus, imparting the chirality of CCQDs to achiral MOFs for creating chiral MOFs is exceptionally attractive to design and assemble novel chiral MOF-based materials.

In the present work, a simple one-pot electrodeposition method was first developed to introduce CCQDs to Cu-TDPAT[11] on nickel foil (MOF@CCQDs/NiF) for the sensitive determination of tyrosine (Tyr) isomers. L-Tyr is an important precursor for neurotransmitter synthesis *in vivo*, such as dopamine, catechins, and norepinephrine.[12] In contrast, D-Tyr could inhibit the nutritional balance in the body.[13] In eosinophils, L-Tyr generates melanin through tyrosinase mediated reaction to prevent vitiligo,[14] and it has a certain therapeutic effect on hyperthyroidism.[15] Thus, the recognition and detection of Tyr enantiomers will be of great importance to study

[a]*School of Chemistry and Chemical Engineering, University of Jinan, Key Laboratory of Interfacial Reaction & Sensing Analysis in Universities of Shandong, Shandong Provincial Key Laboratory of Fluorine Chemistry and Chemical Materials, Jinan 250022, P. R. China. E-mail: chm_kuangx@ujn.edu.cn*

[b]*College of Traffic Civil Engineering, Shandong Jiaotong University, Jinan, 250023, China. E-mail: kuangr1985@foxmail.com*

† Electronic supplementary information (ESI) available: Full synthetic and experimental details, and additional figures and images. See DOI: 10.1039/C9DT04354C

Tyr related medical applications. Cu-TDPAT has been generally researched because of its high porosity and exceptional water and thermal stability.[11] Herein, a Cu-based achiral MOF is used as the scaffold of CCQDs to construct receptor units, where CCQDs not only act as chiral selectors but also promote electronic transmission. This integrated electrode with a uniform and dense film can enantioselectively detect chiral Tyr with high sensitivity because of its different binding strengths resulting from the exposed polar functional groups.

Fig. S1a† shows the TEM image of D-CQDs prepared by a microwave-assisted synthetic approach. The synthesized D-CQDs have a spherical shape and are uniformly dispersed in solution. The distribution of the particle size for the monodisperse NPs ranges from 7 to 10 nm. The optical properties of the D-CQDs shown in Fig. S1b† are measured by UV-vis absorption and fluorescence spectroscopy. One obvious absorption peak at 268 nm with a tail extending into the visible range is ascribed to the $\pi$–$\pi^*$ transition of the $sp^2$-hybridized carbon network.[16] The bright blue luminescence of the D-CQD solution under ultraviolet radiation at 365 nm corresponds to the absorption and emission peaks at 310 and 415 nm,[17,18] respectively.

The surface morphology and structural characterization of MOF@CCQDs/NiF are investigated by SEM, FT-IR, CD and XRD. The successful functionalization of the MOF is first evaluated by FT-IR. As shown in Fig. 1a, the characteristic modes of C–H (stretching vibration at 2939 $cm^{-1}$ and 2893 $cm^{-1}$, bending vibration at 1313),[19] C=O (symmetric stretching vibration at 1712 $cm^{-1}$),[20] C=C (stretching vibration at 1646 $cm^{-1}$) and C–O (stretching vibration at 1083 $cm^{-1}$)[21] belonging to the D-CQDs are observed in the MOF@D-CQD spectrum. It is noteworthy that the absorption peak of the O–H[19] stretching vibration is enhanced and broadened in MOF@CQDs compared with the pure MOF and D-CQDs, which is assigned to the formation of hydrogen bonds between O–H on the surface of the D-CQDs and MOF. An obvious red shift from 3426 $cm^{-1}$ to 3376 $cm^{-1}$ for O–H and from 1720 $cm^{-1}$ to 1712 $cm^{-1}$ for C=O in MOF@CCQDs also confirms the formation of hydrogen bonds. For further confirmation, the XRD patterns of the simulated MOF, synthesized MOF, D-CQDs and MOF@D-CQDs are shown in Fig. 1b. The XRD patterns of the synthesized MOF match well with the patterns of the simulated Cu-TDPAT, but no visible characteristic peak of the D-CQDs around $2\theta$ = 21°, originating from the amorphous carbon,[22] is observed on the MOF@D-CQDs, probably because of the high dispersion and the D-CQDs being distributed in the channel of the MOF skeleton, which has been reported in other studies as well.[23] These results indicate that the obtained composite maintains the framework of the host MOF. After the formation of MOF@D-CQD, most peaks of XRD patterns are identical to those of the simulated Cu-TDPAT and are a bit rough owing to the change in crystalline interplanar spacing compared with the pure MOF.[24] Some peaks are weakened and even disappear because of the interactions of CQDs with the MOF resulting in the loss of partial crystal faces of the MOF. As illustrated in Fig. 1c, the obvious opposite cotton effects of the MOF@L- and D-CQDs located from 210 nm to 440 nm are distinctly distinguished from Cu-TDPAT, indicating that the chirality of the MOF@L- and D-CQDs does not derive from the MOF. SEM images (Fig. 1d) show the uniform distribution of the MOF@D-CQD monocrystals (~200 nm) with an accurate boundary on Ni foil, leading to the formation of a dense film. No visible trace of the D-CQDs is discerned on these smooth surfaces of monocrystals because of their infinitesimal size.

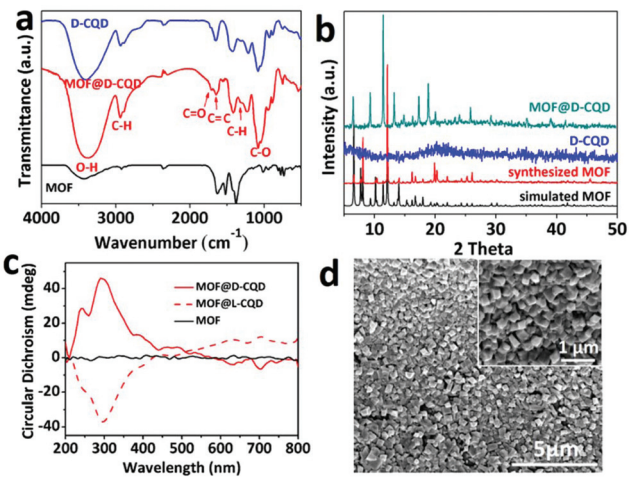


**Fig. 1** (a) FT-IR spectra of MOF (black line), MOF@D-CQDs (red line) and D-CQDs (blue line); (b) XRD patterns of the simulated MOF (black line), synthesized MOF (red line), D-CQD (blue line) and MOF@D-CQDs (green line); (c) CD spectra of MOF (black line) and MOF@D/L-C dots (red line); and (d) SEM images at different amplifications of MOF@D-CQDs/NiF.

Electrochemical impedance spectroscopy (EIS) can provide information about the change in charge-transfer resistance on the surfaces of functionalized electrodes.[25] The Nyquist plots of different electrodes are shown in Fig. S2.† The value of the charge transfer resistance of MOF@CCQD/NiF (61 Ω) is significantly lower than that of MOF/NiF (89 Ω). It can be indicated that the introduction of CQDs significantly improves electrochemical behaviors due to the increasing electrochemical surface area and strong electrostatic interactions between the electrode surface and negatively charged potassium ferricyanide.

The influence of the additional content of chiral CQDs on the recognition of Tyr isomers is investigated since chiral CQDs play a crucial role in enhancing the recognition ability of samples. Fig. S3† shows the recognition ability of a series of MOF@CCQD/NiF samples prepared with different amounts of D-sorbitol (0.15 g, 0.3 g, 0.45 g, 0.6 g), defined as samples 1–4. It has been found that the maximum peak current ratio ($I_D/I_L$) and the potential difference ($\Delta E_p$) of D-Tyr and L-Tyr show a trend of first increasing and then decreasing with an increase in CQD content. It is possible that larger concentrations cause more and more chiral CQDs to agglomerate on the surface of the MOF or in the channel, thereby reducing the active sites of CQDs and the MOF. Thus sample 2 was used in all further studies.

The electrochemical behavior of MOF@CCQD/NiF can be seriously affected by pH. The effect of pH ranging from 5.0 to 8.0 in a 10 mL PBS solution containing 1.2 mM Tyr enantio-

 

mers is studied by cyclic voltammetry (CV). As shown in Fig. 2, the oxidation peaks of D-Tyr and L-Tyr recognition are not obvious in PBS solution (Fig. 2a, b and d). However, there is a distinct peak difference with $I_D/I_L$ = 1.62 and $\Delta E_p$ = 45 mV of D-Tyr and L-Tyr in the 0.1 M PBS solution (pH = 7) (Fig. 2c). Moreover, the oxidation peak potentials of D-Tyr and L-Tyr move to a negative potential with an increase in pH, proving that protons directly participate in the oxidation of Tyr in MOF@CCQD/NiF.

The electrochemical response to different concentrations of Tyr enantiomers using the prepared MOF@CCQD/NiF is investigated by CV curves (Fig. 3). The peak currents are constant with an increasing concentration of D/L-Tyr and there is a linear relationship over the range of 0.2 mM to 1.2 mM. The regression equations are $I_p = 1.082 + 1.649C_L$ ($R^2 = 0.9966$) and $I_p = 0.6101 + 1.030C_D$ ($R^2 = 0.9497$) ($I_p$: mA, $C$: mM). In addition, the detection limits (DL) for D/L-Tyr defined as the concentration, $c_L$, are derived from the smallest measure, $x_L$, that can be determined from the regression equations above (ESI 1.5†). The computed DLs for D and L-Tyr are $6.12 \times 10^{-6}$ and $9.85 \times 10^{-7}$ M, respectively. MOF@CCQD/NiF exhibits good chiral recognition ability towards the D/L-Tyr isomers in this concentration range, demonstrating the successful quantitative determination of Tyr enantiomers.

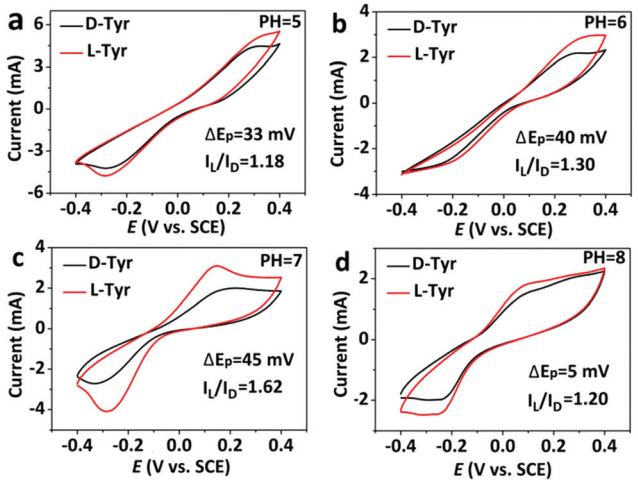


Fig. 2 Differential cyclic voltammetry with a scan rate of 5 mV $s^{-1}$ on 1.2 mM D-Tyr and L-Tyr included with MOF@CCQD/NiF at different pH values: (a) pH = 5.0, (b) pH = 6.0, (c) pH = 7.0 and (d) pH = 8.0.

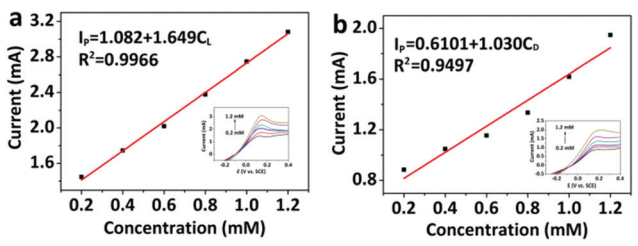


Fig. 3 The plot of current *versus* the concentrations of (a) L-Tyr and (b) D-tyrenantiomer. Inset: CV images of (a) L-Tyr (0.2 mM–1.2 mM) and (b) D-Tyr (0.2 mM–1.2 mM) in the MOF@D-CQDs/NiF electrode in 0.1 M PBS solution.

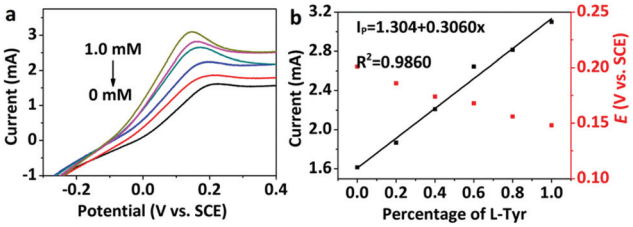


Fig. 4 (a) CVs of 10 mM Tyr enantiomer mixture with different concentrations of L-Tyr (0, 20, 40, 60, 80 and 100%) on MOF@CCQDs/NiF and (b) linear relationship between the current and percentage of L-Tyr.

We further evaluate the chiral recognition ability of the MOF@CCQD/NiF chiral interface in the racemic mixtures of D/L-Tyr (total concentration: 1.0 mM). Fig. 4 presents the CV change of different concentrations of L-Tyr (from 0.0 to 100%) in the racemic mixture. Fortunately, the peak current changes along with the proportions of Tyr enantiomers. Obviously, the peak current is linearly correlated with L-Tyr% and the correlation coefficient is 0.9860. Meanwhile, the peak potential is also linearly correlated with an increasing percentage of L-Tyr in the mixture solution. Since the calibration curves exhibit good linearity, the proposed MOF@CCQD/NiF can be readily determined from one enantiomer of Tyr in the counter isomer. The long-term stability of the developed MOF@CCQD/NiF electrode was also evaluated for practical application (Fig. S4†). After storing at 4 °C for 2 weeks, potential difference and maximum peak current ratio keep 95.6% and 98.8% in 0.1 M PBS solution (pH = 7) with 1.2 mM D-Tyr and L-Tyr. This finding indicates that MOF@CCQD/NiF shows satisfactory stability and reproducibility for chiral recognition.

In summary, an innovative strategy is applied for designing an integral chiral MOF@CCQD/NiF electrode with outstanding selectivity and good sensitivity towards Tyr enantiomers owing to the highly interconnected network architecture of the MOF along with more chiral sites exposed on the surface of the porous skeleton. Moreover, pH sensitivity, chiral selectivity and the ability to determine L-Tyr% in the racemic mixture of the proposed MOF@CCQD/NiF are also discussed in this work. These findings indicate promising stereoselective electroanalytical and electrocatalytic applications.

## Conflicts of interest

There are no conflicts to declare.

## Acknowledgements

This work was supported by the National Key Scientific Instrument and Equipment Development Projects of China (No. 21627809) and the National Natural Science Foundation of China (21605058, 21575050 and 21375047).

## Notes and references

1 (*a*) G. A. Hembury, V. V. Borovkov and Y. Inoue, *Chem. Rev.*, 2008, **108**, 1–73; (*b*) P. Li, Y. He, J. Guang, L. Weng, J. C. G. Zhao, S. Xiang and B. Chen, *J. Am. Chem. Soc.*, 2014, **136**, 547–549; (*c*) H. Su, Q. Zheng and H. Li, *J. Mater. Chem.*, 2012, **22**, 6546–6548.
2 J. M. Brown and S. G. Davies, *Nature*, 1989, **342**, 631–636.
3 R. P. Liang, C. M. Liu, X. Y. Meng, J. W. Wang and J. D. Qiu, *J. Chromatogr. A*, 2012, **1266**, 95–102.
4 K. Hamase, A. Morikawa and K. Zaitsu, *J. Chromatogr. B: Anal. Technol. Biomed. Life Sci.*, 2002, **781**, 73–91.
5 S. O. Kelley, *Sci. Am.*, 2015, **313**, 48–51.
6 A. Zehnacker and M. A. Suhm, *Angew. Chem., Int. Ed.*, 2008, **47**, 6970–6992.
7 C. H. Deng, T. Li, J. H. Chen, J. G. Ma and P. Cheng, *Dalton Trans.*, 2017, **46**(21), 6830–6834.
8 F. Copur, N. Bekar, E. Zor, S. Alpaydin and H. Bingol, *Sens. Actuators, B*, 2019, **279**, 305–312.
9 L. Hu, Y. Sun, Y. Zhou, L. Bai, Y. Zhang, M. Han, H. Huang, Y. Liu and Z. Kang, *Inorg. Chem. Front.*, 2017, **4**, 946–953.
10 Y. Zhang, L. Hu, Y. Sun, C. Zhu, R. Li, N. Liu, H. Huang, Y. Liu, C. Huangand and Z. Kang, *RSC Adv.*, 2016, **6**, 59956–55996.
11 B. Y. Li, Z. J. Zhang, Y. Li, K. X. Yao, Y. H. Zhu, Z. Y. Deng, F. Yang, X. J. Zhou, G. H. Li, H. H. Wu, N. Nijiem, Y. J. Chabal, Z. P. Lai, Y. Han, Z. Shi, S. H. Feng and J. Li, *Angew. Chem., Int. Ed.*, 2012, **51**(6), 1412–1415.
12 S. I. Resnick, L. Hernandez, J. Chen and B. G. Hoebel, *Pharmacology*, 1978, **17**(3), 157–162.
13 M. Friedman and C. E. Levin, *Amino Acids*, 2012, **42**(5), 1553–1582.
14 Y. Jiang, K. Hu, W. Xie, G. Zheng, J. Sun, Y. Zheng and H. Huang, *Oncol. Lett.*, 2014, **7**(2), 419–422.
15 M. E. Garcia-Melendez, M. Salinas-Santander, C. Sanchez-Dominguez, H. Gonzalez-Cardenas, R. M. Cerda-Flores, J. Ocampo-Candiani and R. Ortiz-López, *Exp. Ther. Med.*, 2014, **8**(5), 1433–1437.
16 H. T. Li, X. D. He, Y. Liu, H. Huang, S. Y. Lian, S. T. Lee and Z. H. Kang, *Carbon*, 2011, **49**, 605–609.
17 L. Xiao, Y. Wang, Y. Huang, T. Wong and H. D. Sun, *Nanoscale*, 2017, **9**, 12637–12646.
18 L. Xiao and H. D. Sun, *Nanoscale Horiz.*, 2018, **3**, 565–597.
19 S. J. Zhu, Q. N. Meng, L. Wang, J. H. Zhang, Y. B. Song, H. Jin, K. Zhang, H. C. Sun, H. Y. Wang and B. Yang, *Angew. Chem., Int. Ed.*, 2013, **52**, 3953–3957.
20 S. Kumar, A. K. Rai, S. B. Rai, D. K. Rai, A. N. Singh and V. B. Singh, *J. Mol. Struct.*, 2006, **791**, 23–29.
21 Z. Ma, H. Ming, H. Huang, Y. Liu and Z. H. Kang, *New J. Chem.*, 2012, **36**, 861–864.
22 Y. Guo, L. Zhang, X. Liu, B. Li, D. Tang, W. Liu and W. Qin, *J. Mater. Chem. A*, 2016, **4**, 4044–4055.
23 Z. Liu, X. Kuang, X. Sun, Y. Zhang and Q. Wei, *J. Electroanal. Chem.*, 2019, **846**, 113151.
24 W. W. Yu and X. G. Peng, *Angew. Chem., Int. Ed.*, 2002, **41**, 2368–2371.
25 Y. Kong, X. Chen, W. Wang and Z. Chen, *Anal. Chim. Acta*, 2011, **688**, 203–207.